

Phys Enph 479/879 Assignment 2

Solving the Time-Dependent Schrödinger Equation using the Space-Discretized Leapfrog-Technique

Jane Cohen^{1,*}

¹*Department of Physics, Engineering Physics and Astronomy,
Queen's University, Kingston, ON K7L 3N6, Canada*

(Dated: February 15, 2024)

This paper explores the computational solution of the Time Dependent Schrödinger Equation Equation (TDSE), a fundamental equation in quantum mechanics that describes the evolution of quantum systems. Through the use of atomic units, we simplify the classical TDSE to employ numerical solutions for various quantum mechanical systems including free space propagation, a simple harmonic oscillator, and a double well potential. Utilizing space discretization and the Leapfrog technique, a symplectic integrator known for conserving system energy, the wave function is found over time for a fixed spatial domain. This study demonstrates the application of sparse matrix multiplication and array slicing methods to efficiently solve the discretized TDSE, comparing their effectiveness and computational speed. Through detailed analysis, we observe the behaviour of quantum systems under different potentials, including quantum tunneling in a double well potentials by varying the system parameters. This investigation not only highlights the importance of computational techniques in solving the TDSE but also provides insights into the quantum dynamics of particles, contributing to our understanding of quantum mechanics and its applications in physical systems.

I. INTRODUCTION

In the field of quantum mechanics, the behaviour of quantum systems can be modelled by the Schrödinger Equation, a foundational equation that provides a description of the dynamics of particles at the quantum level [1]. This paper outlines the use of the Time Dependent Schrödinger Equation (TDSE) and explores its applications through a computational lens. Through the use of atomic units to simplify the classical form of the TDSE, this equation is solved for various quantum mechanical systems. The introduction of space discretization allows the numerical solution of the TDSE to be found as we step through time and predict the evolution of wave functions in a fixed spatial domain. This paper also explores the application of symplectic integrators, specifically the Leapfrog technique, which is known for conserving the total energy of the system, to solve the discretized TDSE. Through this approach, the wave function remains normalized over time, ensuring the physical validity of the simulations. By employing this method of integration to solve the TDSE, the quantum dynamics of free space propagation, harmonic oscillators, and double well potentials are explored.

II. THEORY

A. Space Descretized Time Dependent Schrödinger Equation

A quantum mechanical system's wave function can be described by the Time Dependent Schrödinger Equation (TDSE) as it evolves in time and space. The classical form of the TDSE shown in Equation 1 can be simplified by

using atomic units (a.u.). With these units being used, which is equivalent to setting $\hbar = m_e = e = 1$, the TDSE simplifies to the form shown in Equation 2.

$$-\frac{\hbar^2}{2m} \frac{\partial \psi(x,t)}{\partial x^2} + V(x,t)\psi(x,t) = i\hbar \frac{\partial \psi(x,t)}{\partial t} \quad (1)$$

$$-\frac{1}{2} \frac{\partial \psi(x,t)}{\partial x^2} + V(x,t)\psi(x,t) = i \frac{\partial \psi(x,t)}{\partial t} \quad (2)$$

When solving a partial differential equation such as the Schrödinger equation, we can use a known initial condition and then solve the equation incrementally by stepping through time or space. In our case, we will be stepping through time to predict how the wave function behaves in time for a fixed set of positions. The initial condition will therefore always have the form $\Psi(x,0)$. To allow the solution to the TDSE to be found at each time step, space discretization is used as seen in Equation 3.

$$x_j = jh, j = 0, 1, 2, \dots, N \quad (3)$$

Employing the space discretization to the TDSE, we get a new form shown in Equation 4.

$$\frac{d\psi_j(t)}{dt} = \frac{i}{2h^2} (\psi_{j+1}(t) - 2\psi_j(t)) - iV_j(t)\psi_j(t) \quad (4)$$

We now have $N-1$ coupled differential equations, which can be solved using a number of different ODE solvers. For the evolution of the wave function over time, a symplectic integrator is a suitable type of solver because it conserves the total energy of the system [2]. More specifically, the Leapfrog technique, an example of a symplectic integrator, is used to solve the space-discretized TDSE. Using this method, the wave function remains normalized as it

* 18jpcw@queensu.ca

evolves.

To be suitable for the Leapfrog integrator, the Schrödinger equation must of the general form shown in Equation 5.

$$\frac{dx}{dt} = v, \frac{dv}{dt} = a \quad (5)$$

To get the TDSE into this form, we write the discretized form of the TDSE in terms of the real and imaginary parts of the wave function shown in Equation 6. This version of the TDSE, given by Equation 7a and 7b, now satisfies the form required to use the Leapfrog method.

$$\psi_j(t) = R_j(t) + iI_j(t) \quad (6)$$

$$\frac{dR_j}{dt} = -\frac{1}{2h^2} I_{j-1} + \left(\frac{1}{h^2} + V_j\right) R_j - \frac{1}{2h^2} I_{j+1} \quad (7a)$$

$$\frac{dI_j}{dt} = \frac{1}{2h^2} R_{j-1} - \left(\frac{1}{h^2} + V_j\right) R_j + \frac{1}{2h^2} R_{j+1} \quad (7b)$$

Solving this equation throughout time for a fixed spatial domain will give a description of the wave function of a quantum mechanical system. To complete the description, the periodic behaviour of the system must be considered by ensuring the boundary conditions in Equation 8 are satisfied.

$$\psi_{N+1} = \psi_0, \psi_{-1} = \psi_N \quad (8)$$

B. Virial Theorem

The Virial theorem is a relationship between the total kinetic energy and the potential energy of a system. Systems that are bound by a conservative force are expected to satisfy this theorem, given by Equation 9, where $\langle T \rangle$ and $\langle V \rangle$ are the expectation values for momentum and kinetic energy respectively.

$$2\langle T \rangle = n\langle V \rangle \quad (9)$$

The integer n is given by the power of the interparticle distance for a potential of the form $V(x) = \alpha r^n$.

For a wavefunction $\psi(x, t)$, the expectation values for T and V are given by Equation 10 and 11. These values are averaged over the time cycles to obtain a scaled value.

$$\langle T \rangle = \frac{\hbar^2}{2m} \int_{-\infty}^{\infty} \left| \frac{\partial \psi(x, t)}{\partial x} \right|^2 dx \quad (10)$$

$$\langle V \rangle = \int_{-\infty}^{\infty} V(x) \psi^*(x, t) \psi(x, t) dx \quad (11)$$

III. METHOD

To use the Leapfrog integrator to find the wave function over time, two different techniques were used to find the derivatives of $R_j(t)$ and $I_j(t)$. These two methods, sparse matrix multiplication and array slicing, were chosen to exploit different computational techniques.

A. Sparse Matrix Method

To simplify Equations 7a and 7b, the real and imaginary parts of the wave function can be written as column vectors \vec{R} and \vec{I} . In addition, the coefficients of the equations can be defined explicitly to allow the complete expressions to be written as a multiplication of the column vectors with matrix A . Equation 12 shows \vec{R} , \vec{I} and A where $a_j = \frac{1}{h^2} + V_j$ and $b = -\frac{1}{2h^2}$.

$$\vec{R} = \begin{bmatrix} R_0 \\ R_1 \\ \vdots \\ R_N \end{bmatrix}, \vec{I} = \begin{bmatrix} I_0 \\ I_1 \\ \vdots \\ I_N \end{bmatrix}, A = \begin{bmatrix} a_0 & b & & & \\ b & a_1 & b & & \\ & \ddots & \ddots & \ddots & \\ & & b & a_N \end{bmatrix} \quad (12)$$

Using the definitions above for \vec{R} , \vec{I} and A , the discretized TDSE is re-written in Equation 13.

$$\frac{d\vec{R}}{dt} = A\vec{I}, \frac{d\vec{I}}{dt} = -A\vec{R}, \quad (13)$$

This form of the TDSE satisfies the criteria outline by Equation 5, meaning it can be used with the Leapfrog integrator.

To satisfy the boundary conditions of the system the last element in the first row and the first element in the last row are set as b . This modification creates a “wrap-around” effect that enforces the periodicity of the system.

To increase the speed of the matrix multiplication, the Scipy sparse matrix package is used. Because the matrix A consists of mainly zeros, using functions for sparse arrays allows for matrix multiplication to occur faster.

B. Array Slicing Method

An alternative to the matrix multiplication solution provided above, slicing \vec{R} and \vec{I} strategically allows the derivatives $\frac{d\vec{R}}{dt}$ and $\frac{d\vec{I}}{dt}$ to be found at each step of the Leapfrog integration. Using Equation 7a and 7b, these derivatives are computed directly using \vec{R} and \vec{I} from the previous time step. Instead of implementing the boundary conditions once at the start, as was done for the matrix multiplication method, the boundary conditions are applied at each time step.

IV. RESULTS

A. Free Space Propagation

The first quantum system explored was a free space propagation problem. In this example, the initial conditions $x_0 = -5$, $\sigma = 1$ and $k_0 = 5$ were used to determine the initial wave form given by Equation 14. x_0 , σ and k_0 represent the centre of the initial Gaussian waveform, the width of the Gaussian and the initial momentum of the system. The potential used was $V(x) = 0$, which has no effect on the system. Because there is no potential, the non-zero initial momentum, k_0 , is crucial for there to be any movement in the system.

$$\psi(x, 0) = (\sigma\sqrt{\pi})^{-\frac{1}{2}} \exp\left[-\frac{(x - x_0)^2}{2\sigma^2}\right] + ik_0x \quad (14)$$

Using the space-discretized Leapfrog integrator, the probability density of the wavefunction is shown in Figure 1 at multiple time intervals. The wave packet at each time interval represent the wave function of the system at that given time step for all values of x . Over time, the amplitude of the wave form decays, while the width of the curve increases: the wave function remains normalized. As time increases, the wavefunction also moves from the left of the plot to the right. This movement can be seen by the direction arrows in Figure 1. Once the wave packet reaches the right side, it reappears on the left side of the screen, as seen with the $t=13000$ packet. This periodic behaviour is due to the implementation of boundary condition described in Section II.

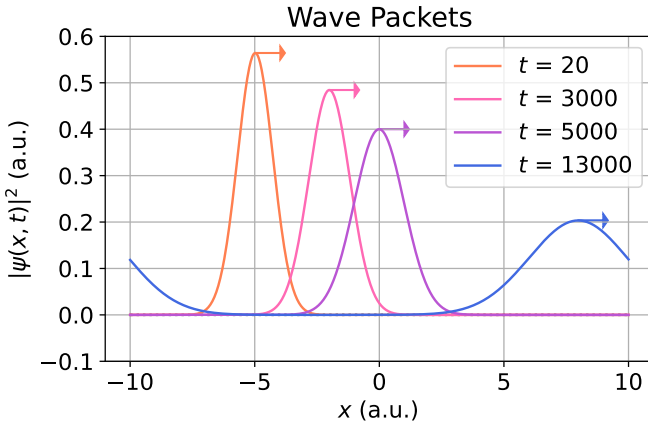


Figure 1. The wavefunction for free space propagation at four time stamps. The system begins with the largest amplitude, before moving to the right as its height decreases and width increases. The arrows on each peak show the direction that the wave packet is moving. The wavefunction remains normalized over time and adheres to periodic boundary conditions. When the wave packet reaches the right hand side of the plot, it appears again on the left side. The simulation was ran for a total of 15000 time steps.

A contour plot, shown in Figure 2, demonstrates the probability density as a function of space and time. This

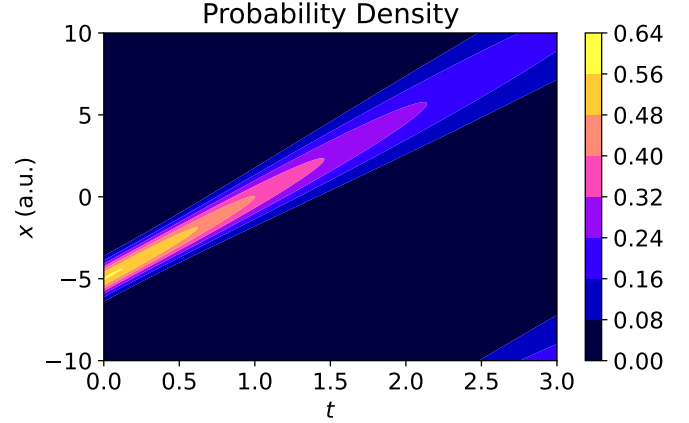


Figure 2. The probability density function for free space propagation. The function is seen to move linearly through space. As time increases, the probability density decreases, shown by a decrease in intensity on the plot. Periodic boundary conditions ensure that when the function reaches an edge of the plot, it returns on the opposite side.

| Run time for derivative calculators | | |
|-------------------------------------|-------------|-------------|
| Method | 1000 points | 2000 points |
| Splicing | 1.99 s | 3.20 s |
| Full matrix | 133.58 s | 625.79 s |
| Sparse matrix | 6.20 s | 8.65 s |

Table I. The run times of methods used to find the derivatives of the real and imaginary parts of the wave function for 15,000 time steps. The methods used were array slicing and matrix multiplication using a full and sparse matrix. The array slicing was the fastest method for both 1000 and 2000 space points.

plot demonstrates the predicted position of the wave function which can be seen to move through space along the vertical axis throughout time. Once the function exceeds the upper limit of this axis, it reappears at the bottom of the screen. Again, this behaviour is due periodic boundary conditions implemented.

For the free space propagation problem, the Leapfrog technique was employed using the slicing method and two matrix multiplication methods. The speed of each method for 15,000 time steps is shown in Table I. The slicing method found the derivatives of \tilde{R} and \tilde{I} for 1000 and 2000 spatial points in the fastest amount of time. In terms of the matrix multiplication techniques, both a full matrix and sparse matrix were used. Using a sparse matrix was significantly faster than a full matrix, especially when the number of spatial points being used was increased. However, both types of matrices were slower than using splicing.

B. Harmonic Oscillator

For a harmonic oscillator with a potential given by Equation 15, the wave function can be solved for using the Leapfrog integrator. For this system, the slicing method was used because if its speed. For the initial conditions $x_0 = -5$, $\sigma = 0.5$ and $k_0 = 5$, the behaviour of the wave packets for two periods of the oscillator are shown in Figure 3.

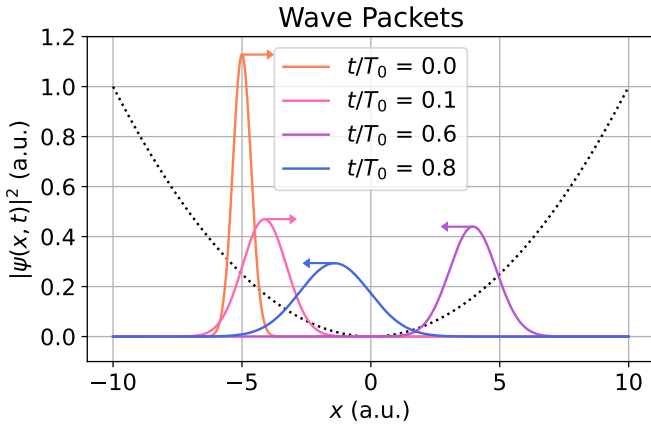


Figure 3. The wavefunction of a simple harmonic oscillator at four time steps. The potential of the system is shown with a dotted black line. The wave packet begins on the left side of the potential well and moves to the other side as time increases. Once it reaches the right side, it changes direction and moves back toward the left. Over many periods, this results in a ‘sloshing’ motion of the wave packet in the potential well.

The potential is also plotted to demonstrate its effect on the wave form. As the potential increases, the amplitude of the wave form follows suit. Visually, it appears as though the wave packet is “sloshing” back and forth between the walls of the potential well.

$$V(x) = \frac{1}{2}x^2 \quad (15)$$

The contour plot, shown in Figure 4, emphasizes the periodic behaviour of the wavefunction. As time increases on the horizontal axis, the potential of the waveform is seen to move from the minimum of the spatial domain to the maximum, before returning again to the minimum.

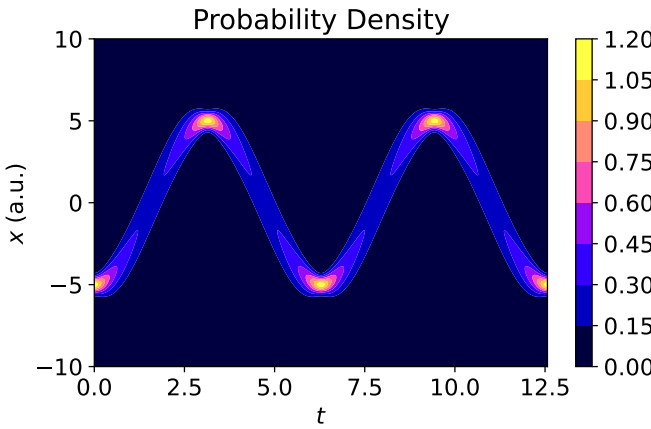


Figure 4. The probability density function of a simple harmonic oscillator in space and time. The system is seen to undergo harmonic motion between the two spatial boundaries. At the peaks of the curves, where the potential is highest, the probability density is highest.

For the harmonic oscillator, the Virial theorem can be evaluated with $n = 2$ due to the square term in the poten-

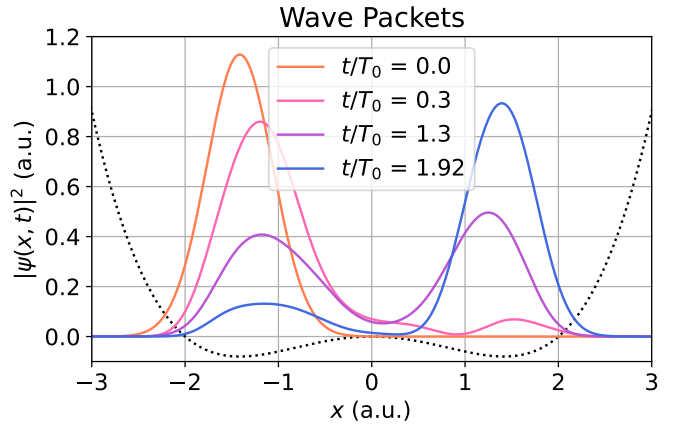


Figure 5. The wavefunction for a double well potential at four time stamps. The potential is shown using a black dotted line. Over time, the amount of the wave function that exists in the right well increases, demonstrating the occurrence of quantum tunneling.

tial. Using this value of n in Equation 9, both sides of the equation are equal to 13.5. The theorem was expected to hold because this system has no dampening, and a symplectic solver was used, resulting in conservation of energy and momentum.

C. Double Well Potential

To explore the behaviour of a double well, the potential given by Equation 16 was used. The initial conditions $x_0 = -\sqrt{2}$, $\sigma = 0.5$ and $k_0 = 0$ were used. Because there is a non-zero potential, no initial momentum is required to observe the behaviour of the system.

$$V(x) = qx^4 - px^2 \quad (16)$$

The double potential well can be seen in Figure 5. For this example, values of $q = 1$ and $p = 4$ were used. This potential results in a system where the wavefunction can tunnel from one well to the other. The direction of the wave packets have been omitted to highlight the distribution of the wave function between the two wells. At the start of the time period, the wave packet is confined completely to the left well. As time progresses, the probability density function begins to ‘tunnel’ into the right well. After a third of a time period has passed, the effect of tunneling can be seen as some of the wave packet has moved to the right well. The amount of tunneling increases and after one period, the wave packet is split between the two wells. This plot demonstrates the probability that the wave packet exists in either well and is a visual representation of quantum tunneling. If the simulation is run for a longer time, the wave packet is seen to tunnel back into the left well.

A contour plot was used again to show the probability density function over time and space. Shown in Figure 6, the expected position of the wave packet can be seen to exist within the rough barrier of one well, before slowly

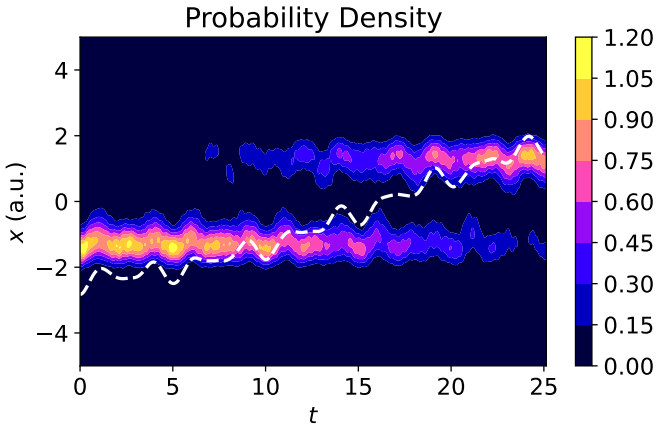


Figure 6. The probability density of a double well potential over space and time. The expectation of the position has been overlayed using a white dashed line. As time increases, the probability density moves from the first well (-1 a.u.) to the second well (1 a.u.). The potential parameters q and p used are 1 and 4.

moving to the other well. The expectation value of x , given by Equation 17 is overlayed on the plot.

$$\langle x \rangle = \int_{-\infty}^{\infty} \psi^*(x, t) x \psi(x, t) dx \quad (17)$$

Varying the parameters p and q directly affects the tunnelling rates of the system. Visually, this is seen as a change in shape of the double well. When the q parameter is increased, it makes the potential well thinner. In other words, it makes the two wells closer together. This transformation allows tunnelling to happen more quickly. Therefore, q is directly proportional to the rate of tunnelling. The p parameter on the other hand, changes the depth of the well. For a larger p , the well is deeper, resulting in longer tunneling times. Therefore, the p parameter is inversely proportional to the rate of tunnelling. These results were determined by observing the time it takes the system to tunnel from one well to the other. These results are an approximation because the exact moment when tunnelling occurs cannot be determined. To obtain the general results, the probability density plots for a range of p and q values were examined. The time when the expectation value moved from one well to the other was deemed the rate of tunnelling. Examples of these probability density plots can be seen in Figure 7. Figure 7 (a) demonstrates the increased rate of tunnelling for a lower value of p as the rate at which the probability density moves between wells is much faster than that in Figure 6. Figure 7 (b) on the other hand, shows that the tunnelling rate increases for a higher value of q .

V. CONCLUSION

This study has explored the behaviour of quantum mechanical systems by employing a computational approach to solve the Time Dependent Schrödinger Equation

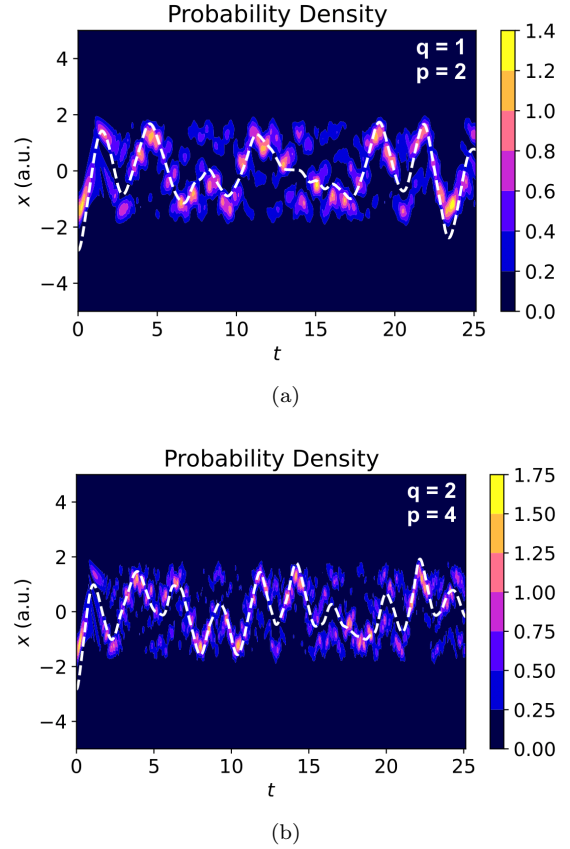


Figure 7. Two probability density function over time and space for a double well potential. The parameters q and p are parameters that change the shape of the potential. These parameters are varied between the two plots to demonstrate their effect on the probability density. Figure (a) shows the function for values of 1 and 2 for q and p respectively. Figure (b) shows the function for values of 2 and 4 for q and p respectively.

(TDSE). Using a simplified form of the TDSE, the effectiveness of symplectic integrators, specifically the Leapfrog technique, was demonstrated. This approach ensured the conservation of energy and the normalization of the wave function throughout the computational process. Using space discretization, the evolution of the wave function for free space propagation, a harmonic oscillator, and a double well potential was successfully displayed. For free space propagation, the use of periodic boundary conditions and the comparison of different computational techniques were employed. It was found that while both sparse matrix multiplication and array slicing are satisfactory techniques for applying boundary conditions, array slicing is a faster method. For the harmonic oscillator, the Virial theorem was tested to demonstrate the conservation of energy and momentum in a system bound by a potential. Lastly, the double well potential was used to explore quantum tunnelling. By varying the parameters of the potential well, the tunnelling times of the system were manipulated. In conclusion, this study has provided insight into the computational and numerical methods that can be employed to gain a deeper understanding of the behaviour of quantum mechanical systems.

VI. REFERENCES

-
- [1] J. E. Osang, I. O. Adedokun, C. Isreal-Cookey, A. O. Egor, U. I. Uquetan, C. M. Ekpo, and J. I. Umuji, “Review of mathematical modelling of the time dependent schrodinger wave equation using different methods,” *Specialty Journal of Engineering and Applied Science* **5**, 10–27 (2020).
 - [2] Denis Donnelly and Edwin Rogers, “Symplectic integrators: An introduction,” *American Journal of Physics* **73**, 938–945 (2005).